Gravity Deformation Measurements of NASA's Deep Space Network 70-Meter Reflector Antennas

W. A. Imbriale,[1] M. J. Britcliffe,[1] and M. Brenner[2]

All of NASA's Deep Space Network (DSN) 70-m reflectors were measured using a Leica TDM-5000 theodolite. The main-reflector surface was measured at five elevation angles so that a gravity deformation model could be derived that described the main-reflector distortions over the entire range of elevation angles. The article describes the measurement equipment and accuracy and the results derived from the data.

I. Introduction

One of NASA's current technology initiatives is to increase deep-space communications capacity by the implementation of 32-GHz (Ka-band) reception on all Deep Space Network (DSN) antennas. A major problem for Ka-band on the 70-m antennas is the loss in gain with elevation angle due to gravity-induced structural mechanical distortions of the main-reflector surface. One of the proposed solutions is to use a deformable flat plate (DFP) in the optics path to compensate for the main-reflector distortions. However, the design of the DFP requires knowing the actual surface shape over all elevation angles. The initial experiment on the 70-m antenna used holographic measurements at three lower elevation angles to predict the surface over the entire elevation range. Holography does not provide a direct measurement of the surface above 47 deg and relies on extrapolation of the lower angle data to predict the surface at high elevation angles. Therefore, the accuracy of the high elevation surfaces is unknown. Also, the measured efficiencies of DSS 14 and DSS 43 as a function of elevation angle as shown in [1] differ significantly. Consequently, Michael Brenner of Engineering Metrology Services (EMS) was contracted to measure the DSS-14, DSS-43, and DSS-63 main-reflector surfaces over the full range of elevation angles using a ranging theodolite. This article describes the measurement equipment and accuracy and the results derived from the data.

---

[1] Communications Ground Systems Section.

[2] Engineering Metrology Services, Tucson, Arizona.

The research described in this publication was carried out by the Jet Propulsion Laboratory, California Institute of Technology, under a contract with the National Aeronautics and Space Administration.

II. Equipment and Accuracy

Most of the measurements described in this article were made using a Leica TDM-5000 "total station" theodolite, as shown in Fig. 1, tied into a portable PC with measurement software. The instrument measures vertical and horizontal angles and distances, downloads them to the PC with MeasTools© [2] software that converts the coordinates from the spherical to a Cartesian system, manages coordinate transformations, and can be used to command the instrument to motor to a desired look angle.

The inherent instrument accuracies are

(1) Angle accuracy, ±1 arcsec

(2) Estimated operator angle accuracy, ±3 arcsec

(3) Distance accuracy with tape targets, ±1.27 mm

During the nighttime measurements, the average temperature was close to 40 deg F. The resulting 27-parts per million (1 mm at the perimeter of the main reflector) distance measurement bias was compensated in software.

III. Targeting

In this procedure, 20-mm-square tape targets 0.3-mm thick (see Fig. 2) were attached to the front face of JPL black plastic targets such that the visible target crosshair was 1.1 mm above and normal to the local reflector surface. The estimated target height variation is on the order of ±0.38 mm.

IV. Measurement Procedure

The theodolite was bolted securely to the bracket close to the center of the main reflector. Its gravity compensator was turned off so that it would rotate with the reflector. Targets were placed in 12 concentric rings wherever cables, supports, or other equipment in the feed support structure did not block the view. Cables were tied back out of the way as much as possible. Figure 3 shows the 367 visible target positions

Fig. 1. Leica TDM-5000 theodolite.

Fig. 2. A single target.

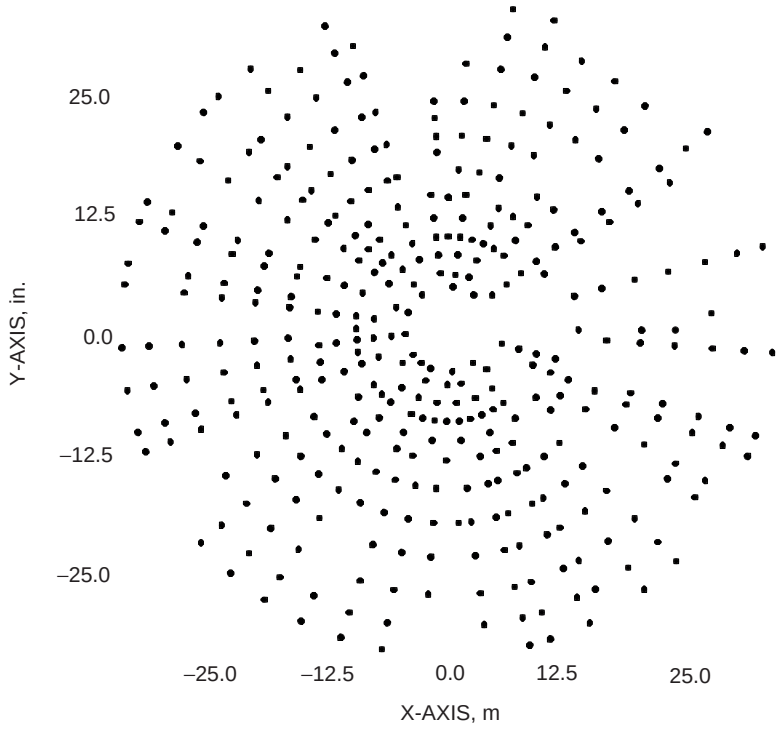

Fig. 3. Visible target placement.

on DSS 14 for the zenith measurements. A similar set of targets was used for the other antennas. The view in the figure is as the targets might appear facing the reflector surface with the main reflector at horizon. A picture of some of the targets on DSS 14 is shown in Fig. 4. At other angles, fewer targets were visible due to movement of feed structure cable bundles as the reflector rotated to a new position.

V. Measurement Error

The total station theodolite measures distance and angle measurements from the instrument to the target on the reflector surface. The measurement geometry is shown in Fig. 5. The range and angle data are used to compute the error normal to the reflector surface for surface adjustment or to half-path-length error (HPLE) for antenna-efficiency calculations.

The major error contributors are the angle reading error, distance measurement error, and targeting error. By viewing a target as closely as possible to tangent to the surface, the effect of distance measure-

Fig. 4. Multiple targets on DSS 14.

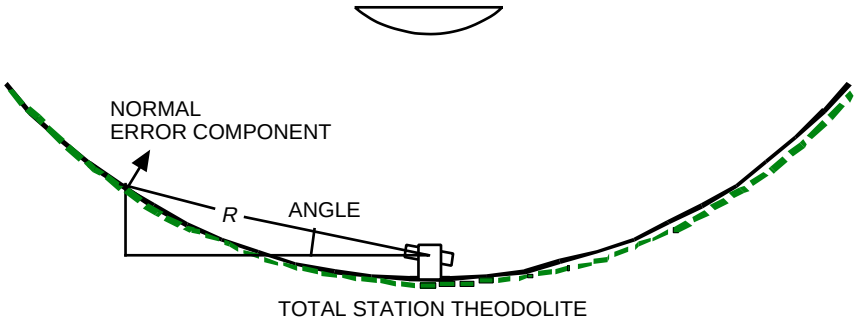

Fig. 5. Reflector measurement geometry.

ment error inherent in the theodolite is minimized. The farthest target is 36.44 m from the vertex of the main reflector. Using this distance with the estimated operator angle accuracy of ±3 arcsec gives a peak surface-normal measurement error of ±0.53 mm.

For a parabolic main reflector with a theodolite at the vertex, the slope of the theodolite line of sight to any target is half of the parabola surface slope at the target. For this shaped main reflector with a nominal focal length of 27 m, the edge slope at a 35-m radius is 33 deg, so the reflector surface is tilted by as much as 16.5 deg to the theodolite line of sight. Based on a distance measurement error of 1.27 mm, this component of the measurement error is $1.27 \tan(16.5 \text{ deg}) = \pm 0.38$ mm.

In addition, it is estimated that target height variation is on the order of ±0.38 mm.

Figure 6 shows the estimated 1-sigma measurement error normal to the surface as a function of distance from the instrument to the target. The angle, range, and targeting-error components are shown with the rss total and the area-weighted 1-sigma rms HPLE of 0.17 mm.

This error estimate is for the absolute accuracy of the measurement. The error in a surface with accuracy better than 0.17 mm rms could not be resolved. This is also the limit of the accuracy that could be achieved by adjusting a surface with a higher rms using data from these measurements.

For differential measurements such as studies of the effect of gravity deformation on antenna efficiency, where the measured difference is taken for the entire reflector, the resolution is much higher. The errors in angle and distance tend to cancel. The targeting error cancels directly. This is verified by the standard deviation of 0.07 mm for three measurements of DSS 14 at an elevation angle of 89 deg. This is the best estimate of the resolution for differential changes of the entire reflector.

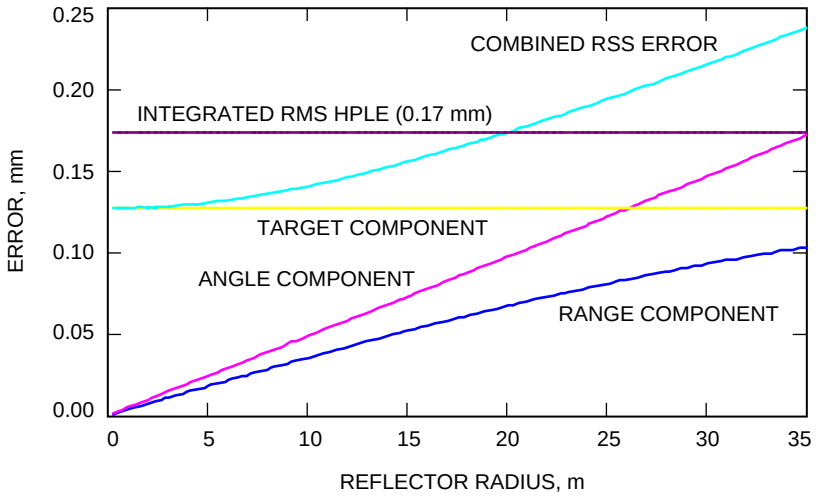

Fig. 6. Measurement error (1 sigma).

VI. Coordinate Systems and Data Analysis

The targets in the reflector coordinate system are shown in Fig. 3. The x-axis is horizontal and parallel to the elevation axis. The y-axis is vertical with the main reflector pointed at horizon. The z-axis is the boresight axis from the vertex to the focus. The reflector coordinate system is based on a reference file created from the nominal target locations. First the nominal target coordinates were calculated based on the measured reflector surface arc length, circumferential spacing, and reflector radial surface shape, and combined into a reference file. The theodolite system motored to the nominal location of each target;

the target was placed precisely in the theodolite crosshairs and then measured and recorded. When all of the targets were measured the first time at zenith, the data were best fit to the theoretical coordinates in the reference file to transform the coordinates from a theodolite-centered coordinate system to the reflector system. No reference points, which might indicate the true reflector optics, were used in any of the measurements. The recorded target locations thus transformed became the new reference target file used in all subsequent measurements.

Subsequent to storing the measured coordinates in the reflector coordinate system, the data were copied into AnTools© [3] software, which fits the measured data points to the theoretical surface of the shaped main reflector, reports residual surface errors, calculates rms accuracy, and provides surface-error plots. Results are presented as half-path-length errors (HPLEs) in millimeters (mm). The HPLE is the usual presentation of surface errors that relates surface rms with gain loss [4].

Table 1 shows the AnTools© calculation of the rms errors after best fitting for DSS 14. The best fitting applied performed a least-squares fit using 6 deg of freedom: translation in the x-, y-, and z-axes, rotation about the x- and y-axes, and focal point adjustment. The first data row is for all measured points. The second row removes the inner panel, which is blocked by the subreflector, and the outer panel, which was not included in the holographic measurement or alignment. Since the AnTools© program was not supplied the correct-as-designed surface for the outer-edge points, the rms using all the points is larger than might be expected.

Table 1. Measured rms errors for DSS 14.

RMS	Elevation angle, deg													
	13		30		47		68		89 no. 1		89 no. 2		89 no. 3	
	RMS	Meas.	RMS	Meas.	RMS	Meas.	RMS	Meas.	RMS	Meas.	RMS	Meas.	RMS	Meas.
All targets, mm	2.03	309	1.88	333	1.96	348	1.83	344	2.01	366	2.03	367	1.91	346
Inner and outer targets removed, mm	1.02	259	1.04	279	0.864	294	1.14	292	1.27	311	1.22	309	1.30	298

An error was later discovered in the 30-deg data, and the data set subsequently was not used to generate an all-angles model.

The other 70-m antenna surfaces also were measured in the same manner, and the data are shown in Table 2. In this case, the correct-as-designed outer-edge points were used in the data analysis.

Two separate nighttime zenith measurements were performed on subsequent nights to determine the measurement repeatability denoted in Table 1 as no. 1 and no. 2. Additionally, the reflector was again measured at zenith, this time during the day, included in Table 1 as no. 3. The data were best fit to the shaped surface as described above, and the residual half-path-length errors were compared. The file shows that, based on 335 points common to the two nighttime measurements, the rms of the difference between them is 0.37 mm, which is consistent with a 0.25-mm rms measurement accuracy applied to two separate measurements.

Table 2. Measured rms errors for all antennas.

RMS	13-deg elevation angle			30-deg elevation angle			47-deg elevation angle			68-deg elevation angle			89-deg elevation angle		
	DSS 14	DSS 43	DSS 63	DSS 14	DSS 43	DSS 63	DSS 14	DSS 43	DSS 63	DSS 14	DSS 43	DSS 63	DSS 14	DSS 43	DSS 63
All targets, mm	1.32	1.30	1.42	—	1.24	1.50	1.19	1.32	1.24	1.52	1.45	1.42	1.62	1.62	1.70
Inner and outer targets removed, mm	1.07	0.97	1.22	—	0.79	1.14	0.84	0.84	0.91	1.07	1.04	1.09	1.27	1.24	1.50

The residual path-length errors are computed relative to an alternative surface that best fits the deformation surface. This is permissible since the important microwave effect is due to phase-error distribution over the surface. Specifically, if the original parabolic surface deforms into another parabolic surface, all rays from the second surface will have the same new overall path length. Since these rays will arrive at the feed with a constant phase, there will be no adverse microwave effect. The alternative surface is defined in terms of five parameters that constitute a rigid body motion and an additional parameter related to a change in the original focal length. However, it is necessary for the subreflector in a dual-reflector system to be moveable. This allows compatible variations in the microwave path geometry established by the fitting parameters. Repointing the reflector can compensate a majority of the rigid-body translations and rotations, but the change in focal length can only be compensated by z-motion of the subreflector. Since, for a given elevation, there is only one position of the subreflector that can be set and it is typically determined by nighttime conditions, the daytime data need to be fit using the nighttime focal length. If the data for all three cases were fit using the six parameters, then the rms would be 1.65, 1.61, and 1.67 mm, respectively. However, if the daytime data were fit with only five parameters and the focal length held constant to each of the two nighttime measurements, the rms would be 2.29 and 2.49 mm, indicating a rather large focal-length change. By contrast, if the second nighttime measurement is fit with only the five rigid-body parameters and the first nighttime measurement focal length, the rms is 1.63 mm, indicating that there was minimal focal-length change. The delta focal length changes computed from the raw data for the three cases are 3.15, 2.03, and 9.5 mm, indicating that the focal-length change for the thermal effects is greater than 6 mm, a substantial effect. The gain loss due to the thermal-induced focal-length change would be on the order of 5 to 6 dB. However, in practice, this focal-length change is probably somewhat compensated for by the expansion of the quadripod legs that also moves the subreflector in the correct direction.

VII. Measurement of Gravity Sag

With minor adjustments to the theodolite and a comfortable working platform for the operator, primary surface and subreflector position measurements as described above can be performed at any elevation angle for a tracking antenna. For antenna structures that behave in a linear elastic fashion, measurements at three separate elevation angles provide sufficient information to determine the relative positions of all targets at any other angle. (A common example of non-linear structural deformation is the bending of bolted flanges.) The process requires the intermediate calculation of the face-up (zenith-pointing) and face-side (horizon-pointing) gravity deformations of the reflector and their subsequent vector superposition. The best results will be achieved if the elevation angles at which measurements are made are well separated, such as 0, 45, and 90 deg. In this case, the analysis was based on 13, 47, and 89 deg.

The gravity deformation of a linear elastic structure at any elevation angle can be derived by vector superposition of the face-up and face-side gravity vectors as

$$\delta = \delta_u \sin\theta + \delta_s \cos\theta$$

$$\delta_s = \text{face-side gravity deformation}$$

$$\delta_u = \text{face-up gravity deformation}$$

The face-up and face-side deformations described here are of the type derived from a computer structural analysis in which gravity is "turned on" from a particular direction. As such, they cannot be directly measured in the real world. For a linear elastic structure that rotates from angle θ_1 to θ_2, the relative deformation, or motion, will be $\delta_2 - \delta_1$, as shown above. For three measurements, two independent linear equations can be written for $\delta_2 - \delta_1$ and $\delta_3 - \delta_1$:

$$\begin{bmatrix} \delta_u \\ \delta_s \end{bmatrix} = \begin{bmatrix} \sin\theta_2 - \sin\theta_1 & \cos\theta_2 - \cos\theta_1 \\ \sin\theta_3 - \sin\theta_1 & \cos\theta_3 - \cos\theta_1 \end{bmatrix}^{-1} \begin{bmatrix} \delta_2 - \delta_1 \\ \delta_3 - \delta_1 \end{bmatrix}$$

Now that δ_u and δ_s are known, for any angle θ, the predicted alignment error at a target is the gravity deformation traveling from a measured reference angle, θ_2, to angle θ superposed onto the actual measured alignment error at the reference angle, δ_θ. This can be expressed as

$$\delta(\theta) = \delta_\theta + \delta_u(\sin\theta_2 - \sin\theta) + \delta_s(\cos\theta_2 - \cos\theta)$$

The gravity deformations of the reflector were analyzed in the steps described below:

(1) After removing the outer and inner rows, the best-fit parameters for each set of measured data were determined. The HPLE (for *all* the data points) after best fitting were stored in text files.

(2) A sorting program was written to extract out the measurement points common to all six data files.

(3) The gravity analysis was performed using the measurement data from elevations of 13, 47, and 89 deg. The predicted HPLE at each of the common points were calculated at 5-deg elevation intervals from 0 to 90 deg, plus 13, 30 (for DSS 43 only), 47, 68, and 89 deg using the actual measured data. By definition, the predictions at 13, 47, and 89 deg perfectly matched the input data.

(4) The above process was repeated, recording the predicted gravity deformations with respect to the nominal rigging angle of 47-deg elevation.

The rms data are summarized in Figs. 7 and 8 for DSS 14 and DSS 43. The curves show that the measured data at 68 deg (and 30 deg for DSS 43) closely match the predicted values. To further emphasize the fact that the gravity predictions from the three-angle data match the data at the other measured angles, Figs. 9 and 10 show the surface plots of the measured data at 30 and 68 deg compared to the predicted data using only the 13-, 47-, and 89-deg data for DSS 43. For 30 deg, the predicted rms was 0.983 mm, and the measured rms was 0.975 mm. For 68 deg, the results were 1.209 and 1.212 mm, respectively. The values are different from those shown in Table 2 because the data were masked to exclude the outer edge and strut blockage.

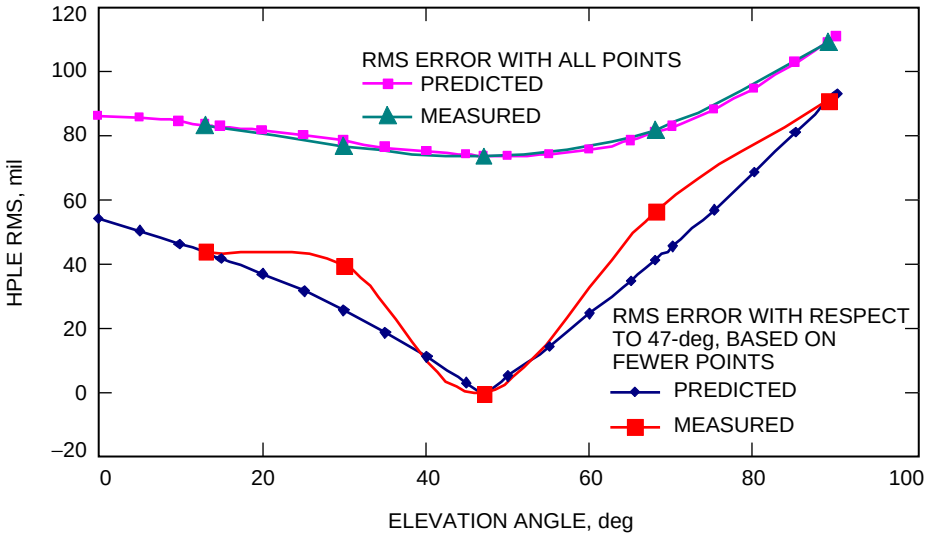

Fig. 7. Summary of predicted versus measured surface rms and gravity deformation for DSS 14.

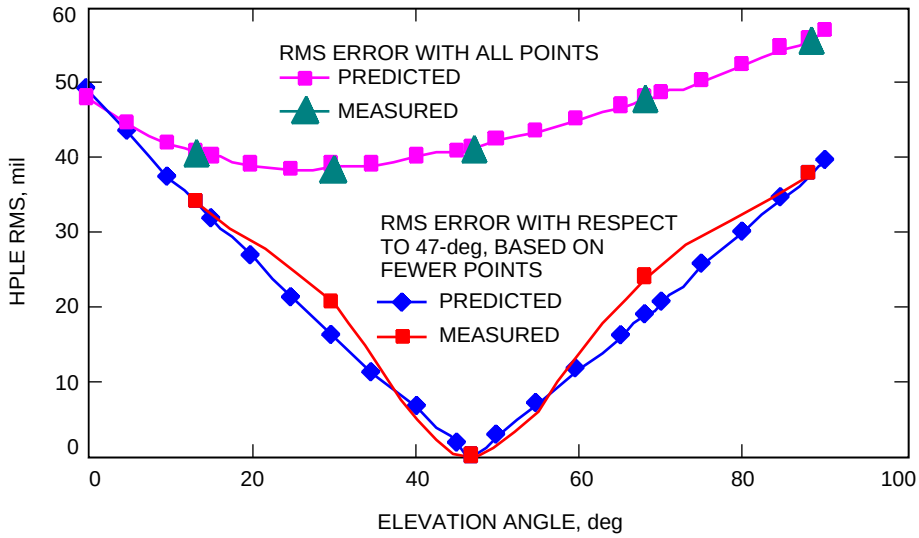

Fig. 8. Summary of predicted versus measured surface rms and gravity deformation for DSS 43.

VIII. Efficiency Calculations and Measurements

Using the all-angle main-reflector surface-shape data in a physical optics calculation with the 70-m feed and subreflector configuration, an efficiency value was determined for all antennas and is shown in Fig. 11. This predicted efficiency value is compared to the measured efficiency at DSS 14 in Fig. 12. This demonstrates that the DSS-43 main-reflector surface gravitational distortion is comparable to DSS 14 and that the measured efficiency difference between DSS 14 and DSS 43 as shown in [1] must be due to other factors, not the main-reflector shape.

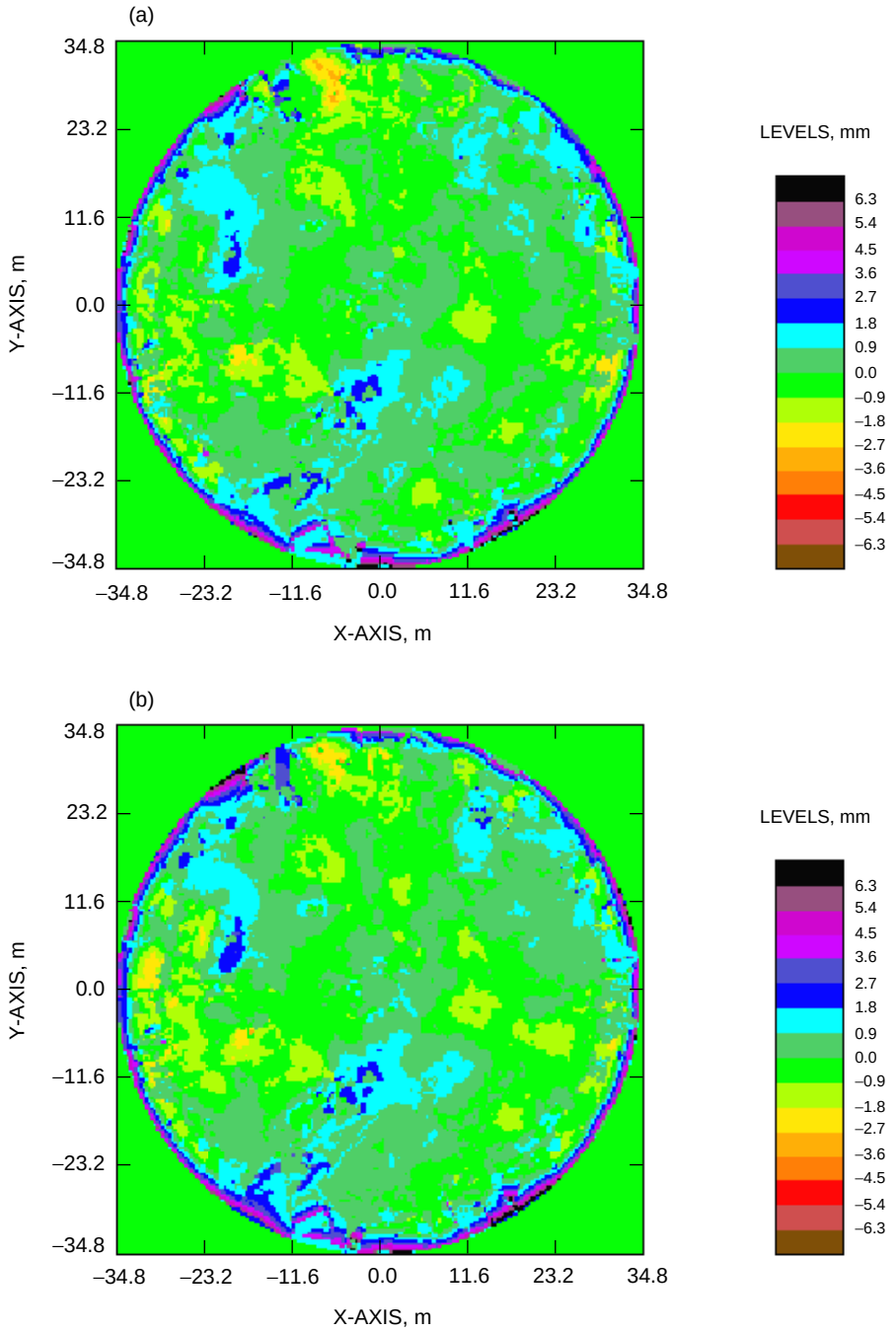

Fig. 9. DSS-43 (a) measured data at 30-deg elevation and (b) reconstructed data using 13-, 47-, and 88-deg elevation data.

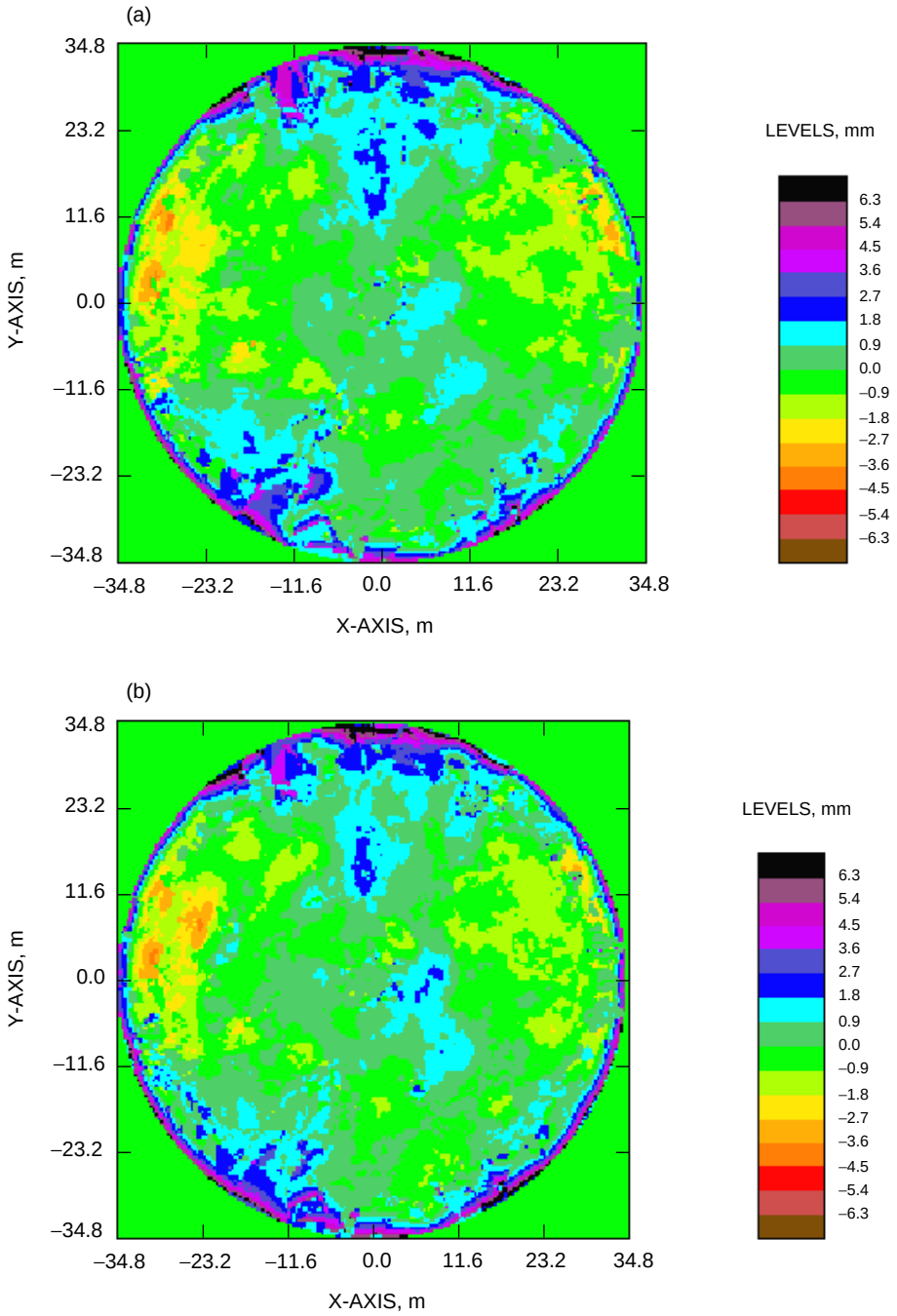

Fig. 10. DSS-43 (a) measured data at 68-deg elevation and (b) reconstructed data using 13-, 47-, and 88-deg elevation data.

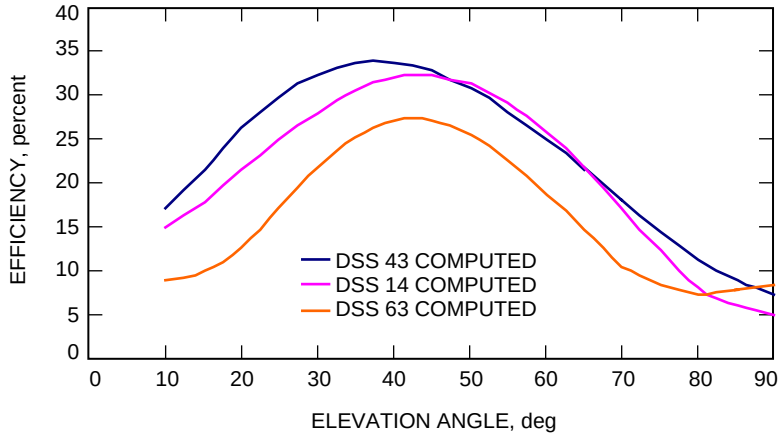

Fig. 11. Computed 70-meter antenna efficiencies, computed from measured surfaces.

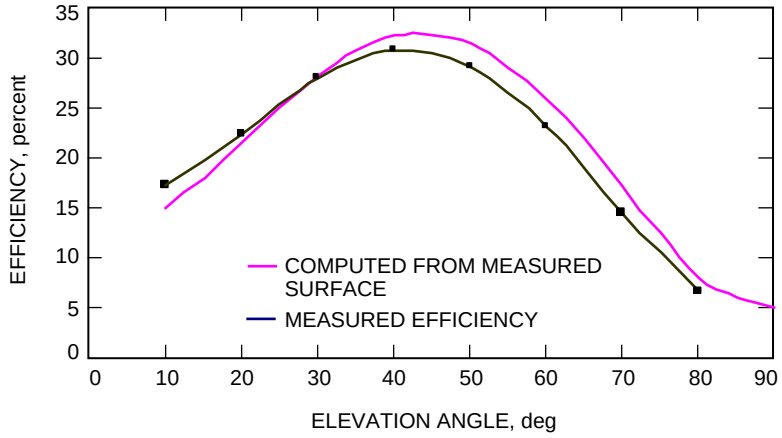

Fig. 12. Computed and measured efficiencies for DSS 14.

IX. Structural Hysteresis Measurement

Previous measurements of the aperture efficiency of DSS 43 at 8.4 GHz (X-band) show some evidence of efficiency difference on tracks of a source rising and setting. The efficiency is different at the same elevation angle depending on whether the source is rising or setting in elevation.

There are several possible causes. Although the antenna is at the same elevation angle, the azimuth angle is different by 90 deg or more. Azimuth dependence has been a problem on beam-waveguide antennas where the antenna moves independently of the feeds. There is no reason to suspect there is an azimuth dependency of the structure on a conventional Cassegrain antenna like DSS 43.

Another possibility is mechanical hysteresis in the tipping structure that causes the reflector to distort differently as the antenna moves up or down. Figure 13 shows the rise–set difference from measured data from DSS 43 on source 0521-365 on day 00/278. At 10-deg-elevation rising, the efficiency is 63 percent compared to 54 percent setting (0.7 dB). At 47 deg, the efficiency rising is 70.5 percent compared to 67 percent setting (0.2 dB).

Figure 14 shows the effect on measured aperture efficiency due to surface rms at 8.4 GHz. The surface rms would need to degrade from 0.86 mm to 0.96 mm at 47 deg to account for the measured efficiency change.

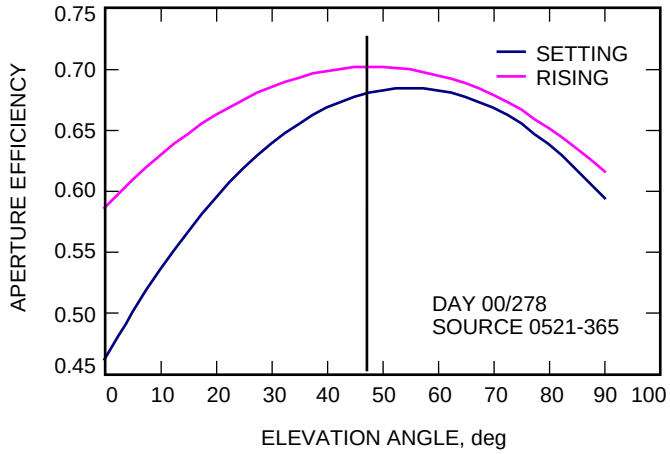

Fig. 13. DSS-43 efficiency at 8.4 GHz for source rising and setting.

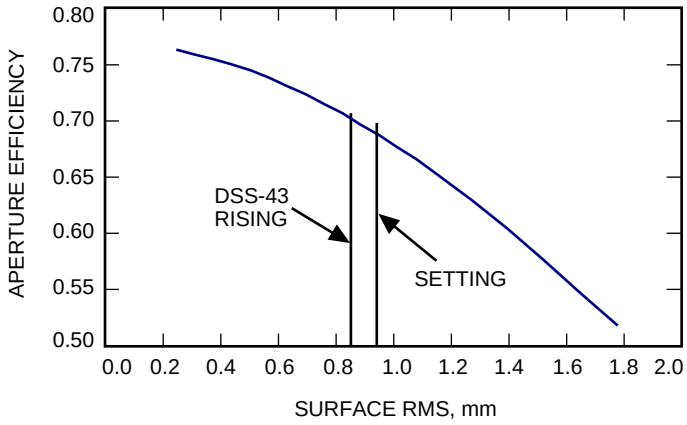

Fig. 14. The effect of surface rms on efficiency for DSS 43 at 8.4 GHz.

An effort was made to identify any mechanical hysteresis in the main reflector by measuring the antenna surface at the same elevation, simulating the antenna motion of a rising versus setting source. The antenna was first measured at 47 deg by moving the antenna from zenith (90-deg elevation) to 47 deg, and again by first moving the antenna to 10 deg, waiting for two hours, and then slowly (0.1 deg/s) moving the antenna up to 47 deg and repeating the measurement. Unfortunately, before the "rising" measurements were completed, the temperature on the main reflector went below freezing during a period of high humidity, and ice formed on the main-reflector targets, making the readings difficult. The schedule did not allow for repeating the measurement. Enough data were collected, however, to suggest that there was no significant difference in the surface rising or setting.

X. Comparison with Holography Data

Holography data at 13-deg elevation were provided as surface-normal errors. The data were masked to remove the inner blocked area, the areas outside the aperture of the dish, and the targets blocked by the spars. Additionally, for consistency, the surface-normal errors were converted into half-path-length errors by multiplying the normals by the cosine of the local slope angle.

The surface plots for both holography and the theodolite measurements are shown in Fig. 15. Visual comparison shows a good match, although some residual errors remain in the outer panels. Statistical

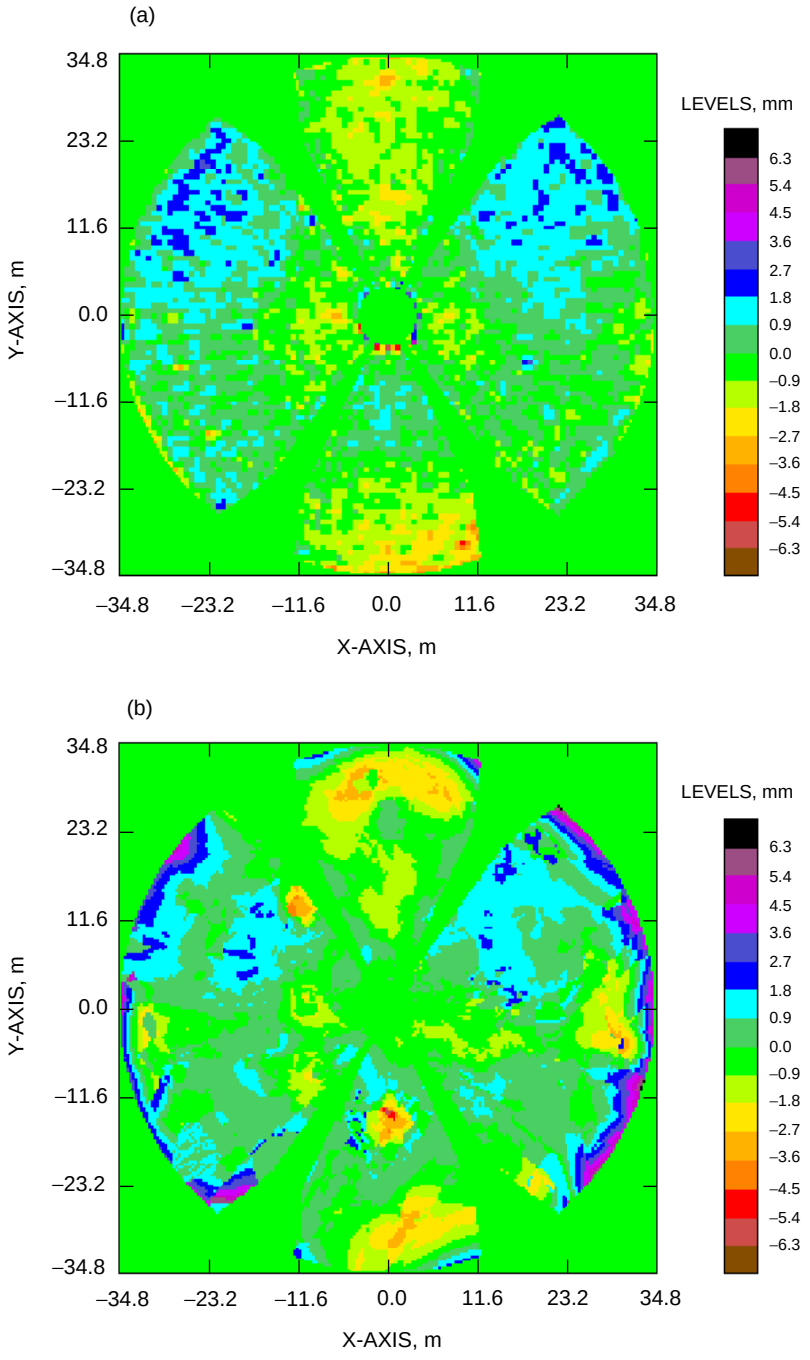

Fig. 15. Comparison of (a) holography and (b) theodolite measurements (struts and center masked).

analysis shows that the holography rms errors are 0.89 mm while the comparable results for the theodolite measurements were 1.04 mm. In view of all of the variables that can account for these differences, this is an adequate match.

XI. Conclusions

The main-reflector surfaces for all three 70-m antennas were measured at 13-, 30-, 47-, 68-, and 90-deg elevation angles, enabling an all-elevation-angle surface-distortion model to be developed. This model is required to design the DFP. The similarity of the distortion data indicates that the same DFP design can be utilized at all three sites. There was good agreement between the measured efficiency of DSS 14 and the computed efficiency from the measured surface data.

Measurements made both during the day and at night indicate that there is a sizable defocusing of the reflector caused by thermal changes. There was no indication of main-reflector surface hysteresis in the measured data. There was good agreement between the theodolite-derived surface measurements and the holography-derived surface.

References

[1] *Deep Space Mission Systems (DSMS) Telecommunications Link Design Handbook*, JPL 810-005, Rev. E, Jet Propulsion Laboratory, Pasadena, California, January 15, 2001.

[2] Engineering Metrology Services, Tucson, Arizona, http://www.engr-metr.com/meastools.html, accessed October 1, 2001.

[3] Engineering Metrology Services, Tucson, Arizona, http://www.engr-metr.com/antools.html, accessed October 1, 2001.

[4] J. Ruze, "Antenna Tolerance Theory—A Review," *Proc. IEEE*, vol. 54, pp. 633–640, 1966.